Unravelling competitive adsorption phenomena in the aqueous phase reforming of carboxylic acids on Pt catalysts: An experimental and theoretical study

Chemical Engineering Journal 482 (2024) 148902

Contents lists available at ScienceDirect

Chemical Engineering Journal

journal homepage: www.elsevier.com/locate/cej

Unravelling competitive adsorption phenomena in the aqueous phase reforming of carboxylic acids on Pt catalysts: An experimental and theoretical study

Giuseppe Pipitone [a,*], Alyssa J.R. Hensley [b,*], Ayodeji Omoniyi [b], Giulia Zoppi [a], Raffaele Pirone [a], Samir Bensaid [a]

[a] Department of Applied Science and Technology, Politecnico di Torino, Corso Duca degli Abruzzi 24, Turin 10129, Italy
[b] Department of Chemical Engineering and Materials Science, Stevens Institute of Technology, Hoboken, NJ 07030, United States

ARTICLE INFO

Keywords:
Aqueous phase reforming
Biorefinery
Density functional theory
Hydrogen
Hydrothermal Liquefaction
Wastewater

ABSTRACT

Biorefinery-derived wastewater is considered a valuable source of energy and chemicals thanks to its organic loading. However, it is constituted by different compounds which influence the performance of a catalytic valorization process. In this work, we investigated the treatment of a synthetic hydrothermal liquefaction-derived wastewater (HTL-WW) via aqueous phase reforming (APR) to obtain hydrogen. As a case study, we examined the underlying driving forces for performance differences in the APR of mono- and bi-component solutions of carboxylic acids as a model corn stover HTL-WW over Pt catalysts via a combined experimental and theoretical approach. In mono-component solutions, the conversion ranked as glycolic acid > propionic acid ≈ acetic acid, and the same was found for the hydrogen production tendency. Binary solutions of glycolic and acetic acid, with different concentration among the constituents, showed a strong inhibition of the acetic acid reactivity due to the prevalent adsorption of glycolic acid on Pt surface. The results from the APR of acetic and propionic acid solutions were less affected by such phenomena. DFT results showed that there are strong, attractive lateral interactions between carboxylic acids due to intermolecular hydrogen bonding that cause all carboxylic acids to preferentially adsorb in dimer structures. The lateral interaction strength was determined for both pure and binary mixtures of carboxylic acid dimers, with results showing that pure mixtures of carboxylic acids have stronger attractions and that glycolic acid dimers see the strongest attractions due to the added terminal hydroxyl functional group. The findings presented herein offer significant insights into the utilization of APR for industrial-like multi-component solutions, as well as for any catalytic process involving small organic compounds in an aqueous phase.

1. Introduction

The sustainable management of water has been targeted as the sixth 2030 Sustainable Development Goal by the United Nations [1]. Apart from municipal wastewater, several industrial sectors, like food processing, as well as biomass-related processes, such as pyrolysis, hydrothermal liquefaction, and hydrothermal gasification, lead to huge amount of contaminated water fractions which need a proper treatment before their release in the biosphere [2]. In this context, the scientific interest has been pushed towards new technologies, in the frame of a carbon circular economy.

The hydrothermal liquefaction (HTL) of wet biomass has the potential to provide renewable biofuels [3]. However, the generated wastewater stream (HTL-WW) cannot be discharged directly as it is an environmental pollutant. Far more important than a wastewater treatment process, it needs a suitable valorization as it can dissolve up to half of the carbon initially present in the feedstock, depending on the reaction conditions [4]. The resources recovery of the aqueous phase could provide economic and energetic benefits to the entire technology, helping in its implementation at a larger scale [5].

So far, two technologies have been typically suggested for the valorization of HTL-WW, specifically, anaerobic digestion and catalytic hydrothermal gasification. The integration between anaerobic digestion and HTL of food waste or algae (among the others) was assessed by

* Corresponding authors.
E-mail addresses: giuseppe.pipitone@polito.it (G. Pipitone), ahensley@stevens.edu (A.J.R. Hensley).

https://doi.org/10.1016/j.cej.2024.148902

Available online 20 January 2024

Posmanik et al. and Fernandez et al. [6,7]. Catalytic hydrothermal gasification was proposed for the HTL-WW valorization of sludge or microalgae [8,9]. Both these processes have interesting performance in terms of carbon removal and energy recovery [10]. Nevertheless, they also have some drawbacks. Anaerobic digestion microorganisms suffer from inhibition due to the presence of certain organic and inorganic compounds, like phenol and ammonia [11]. On the other hand, the catalytic hydrothermal gasification is an expensive process because of the high reaction temperature and pressures required, which impact both the operating and capital costs. Further information on the possible technologies for HTL-WW exploitation can be found in [5,10,12,13].

In this scenario, we recently investigated a catalytic process which shows promising results for the catalytic valorization of HTL-WW, that is aqueous phase reforming (APR). The pioneering work of Dumesic's research group proposed APR due to its possibility to produce H_2 from biomass-derived compounds under milder reaction conditions (220–270 °C, 30–60 bar) compared to conventional fossil-based steam reforming [14]. APR eliminates the need to vaporize water, reducing the energy requirement, and generates a gaseous effluent with low concentration of carbon monoxide in a single reactor, due to the favourable equilibrium for the water gas shift reaction. Thus far, most of the research has focused on single-compound solutions, which were fundamental for the sake of understanding catalyst performance and the influence of operating reaction conditions [15–19]. The influence of the active metals was studied, as well as the support and the preparation procedure, and these aspects were recently reviewed by Pipitone et al. [20].

Critically, there is still a lack of information on the catalytic behaviour of multi-component solutions. The real streams present in industrially relevant environments are constituted by multiple species, belonging to several different classes of compounds (carboxylic acids, alcohols, hydroxyacids, ketones, aromatics, amides, etc.). Therefore, to advance APR (and other catalytic valorization technologies) in the direction of realistic feedstocks, the understanding of the performance for mixtures of reactants becomes of significant importance. In spite of this, the characterization of the feedstock itself is scarce. The Pacific Northwest National Laboratory (PNNL) carried out an experimental campaign where many compounds present in the wastewater by-product were identified and quantified in the case of hydrothermal liquefaction from food waste, algae, municipal or industrial waste [21,22].

In the present work, we took in consideration the work performed by Panisko et al., who reported the composition of the aqueous phase derived from the hydrothermal liquefaction of corn stover [23]. This is one of the most abundant sources of biomass residues, derived from corn production, with high projections of growth both under normal and intensive practices [24]. The authors observed that, after the HTL step, glycolic acid and acetic acid were the main compounds in the HTL-WW, constituting approximately 50 % of the total carbon dissolved in the water fraction, while propionic acid was the second most present carboxylic acid. We reported in a previous work their hydrogen yield in single solutions over a 5 % Pt/Al_2O_3 catalyst [25]. Moreover, preliminary tests with binary mixtures carried out in our laboratory showed that a competition between alcohols, hydroxyacids, and carboxylic acids is possible, but a deeper investigation was required, due to the complexity of real streams.

Therefore, the scope of the present work is the study of the valorization of corn stover HTL-WW via APR using model solutions of a series of carboxylic acids (i.e. acetic acid, propionic acid, and glycolic acid) over a Pt-based catalyst. To the best of our knowledge, this work is the first where the catalytic competitive adsorption issues of complex mixtures, such as the HTL-WW, were systematically tackled using a combined experimental and theoretical approach. Three binary mixtures, constituted by glycolic acid/acetic acid, propionic acid/acetic acid and glycolic acid/propionic acid were investigated to assess the mutual influence of the reactants. Density functional theory (DFT) simulations were performed to rationalize the competitive adsorption behaviours observed experimentally by characterizing the nanoscale interactions between carboxylic acids in pure and mixed systems.

2. Materials and methods

2.1. Materials

Glycolic acid (GA), acetic acid (AA) and propionic acid (PA) were purchased from Sigma Aldrich (reagent grade) and used as received. Deionized water was obtained in the laboratory thanks to a RO Cubic S2 system, whose purification system consists of low-pressure reverse osmosis and ion exchange resins. 5 % Pt/C was obtained by a commercial supplier, in powder form.

2.2. APR test conditions

The APR reactions were performed in a 300 mL 4560 series mini benchtop batch reactor (Parr), equipped with a 4848 model PID controller (Parr). In a typical reaction, 75 mL of solution were used, with the desired concentration of GA, AA or PA (with range being 175–351 mmol/L). A suitable catalyst amount (0.15 g) was used, without any pretreatment, to allow for adequate conversion. Once fastened, the reactor was purged with nitrogen to remove atmospheric oxygen, finally pressurized at 0.3 MPa with N_2, and heated up to the desired temperature (270 °C). Please note that the residence time and the stirring started when the set temperature was reached (ca. 50 min heating time). The absence of external and internal mass transfer limitations was experimentally and theoretically assessed (see Mass transfer analysis paragraph in Supplementary Information). Furthermore, a blank test without any organic compound was carried out to exclude any possible gasification phenomenon of the carbon support. It was observed that the hydrogen production was negligible, corresponding to only 0.1 % of the hydrogen produced in the analogous test using glycolic acid.

At the end of the reaction (with range being 0–3 h), the reactor was cooled down thanks to an internal cooling loop and external water bath. Afterwards, the gas phase was collected in a syringe and analysed by μGC. The liquid phase was filtered by gravity to separate the catalyst and then analysed through HPLC.

2.3. Analytical methods

The gas phase characterization was performed using an SRA MicroGC, equipped with Molsieve 5A (injection temperature equal to 100 °C, argon as carrier, column temperature equal to 85 °C) and PoraPLOT U (injection temperature equal to 90 °C, helium as carrier, column temperature 80 °C) columns, with a TCD detector. The pump sampling time was equal to 20 s, with 40 ms injection time, and 28 psi column pressure. The pressure value at room temperature was used for the quantification of the gas production, using the ideal gas law.

The analysis of the liquid samples was performed through HPLC (Shimadzu), using a Rezex ROA-Organic acid H^+ (8 %) column (300 mm · 7.8 mm). The mobile phase was 0.005 M H_2SO_4 in MilliQ water (18 MΩ/cm, produced in the laboratory). The flow rate was fixed at 0.7 mL/min and the temperature of the column at 50 °C. The injection volume was equal to 10 μL. The products were determined using a refractive index detector (RID) and quantified by external calibration using purchased standards.

Thanks to the data acquired from both instruments, three indicators were defined. These will be used in the following to describe the reaction performance. Eq.1 defines the conversion of the i-th compound at time t, as the ratio between the reacted moles of the component (calculated as the difference of initial – n^i_{in} – and final moles – n^i_{fin}) and the initial moles in the volume mixture; Eq. (2) defines the hydrogen yield as the ratio between the moles of hydrogen obtained at the end of the reaction and the maximum amount of hydrogen that could be produced considering the APR reaction stoichiometry; Eq. (3) defines the gas concentration of

the i[th] component as the ratio between the moles of the component and the total moles of gaseous products.

$$Conversion_i(\%) = \frac{n_{in}^i - n_{fin}^i}{n_{in}^i} \bullet 100 \quad (1)$$

$$H_2yield(\%) = \frac{n_{fin}^{H_2}}{n_{teo}^{H_2}} \bullet 100 \quad (2)$$

$$Gas\ concentration_i(\%) = \frac{n_{gas}^i}{n_{gas}^{tot}} \bullet 100 \quad (3)$$

The apparent reaction order was determined by using a power-law model, by implementing logarithmic linearization and multiple linear regression. The experimental data were fitted using the Solver function in Microsoft Excel, performing a numerical integration of the mass balance equation for the batch reactor model, and minimizing the objective function of the residual squares between model and experimental compound concentration.

The catalyst was characterized to get information regarding its main properties. X-ray diffraction (XRD) analysis was performed to evaluate the crystalline structure of the Pt site. The diffractometer used a Cu Kα source operating at 40 kV and 40 mA. The mean particle size was calculated using the Scherrer's formula from broadening of the associated face-centered cubic (fcc) metal reflections.

The textural properties were obtained by N_2 adsorption/desorption isotherms at 77 K. Prior to the analysis, the samples were pretreated at 200 °C to provide a clean surface for adsorption in a Micromeritics Flow Prep 060 degassing system. The specific surface area was calculated according to the Brunauer-Emmet-Teller (BET) equation, while pore volume and pore size distribution were determined by the Barrett-Joyner-Halenda (BJH) method, in the desorption branch.

XPS measurements were obtained using a PHI Model 5000 electron spectrometer, equipped with an aluminum anode monochromatic source. High resolution spectra were collected by-using a band-pass energy of 11.75 eV. The obtained binding energies were corrected for specimen charging by referencing the C1s = 284.6 eV. The software CasaXPS was used for the analysis and curve fitting of XPS results. The signals for Pt $4f_{7/2}$ and Pt $4f_{5/2}$ were separated by 3.4 eV. The metallic Pt patterns were fitted using an asymmetric line shape LA (1.2, 85, 70), while PtO patterns were fitted by the combination of Gaussian (50 %) and Lorentzian (50 %) functions.

The characterisation of the dispersion of the impregnated metal on the support at the nanoscale was carried out by Transmission Electron Microscopy (TEM) and energy dispersive X-ray spectroscopy (EDX) operated in Scanning-Transmission Electron Microscopy (STEM) mode. A Thermo Fisher Talos F200X TEM/STEM operated at 200 kV equipped with 4 in-column SDD Super-X detectors for elemental maps acquisition was used. The specimens were prepared by sonication of the powder sample in high purity propan-2-ol then drop-casted on holey-C film-coated Cu grids (3.05 mm diam. 300 mesh, TAAB). HAADF-STEM image was analyzed by ImageJ software, counting 245 particles to determine the average size and its distribution.

2.4. DFT calculations

DFT calculations were performed using the Vienna *Ab Initio* Simulation Package (VASP) [26,27] with the core electrons treated using the projector-augmented wave (PAW) [28,29] method (version 54 potentials). The electron-electron exchange-correlation was captured with the optB88-vdW functional [30,31], and electron smearing was modelled with the Methfessel-Paxton [32] (N = 1) method with a width set to 0.1 eV. Ground state optimizations used a plane-wave basis set with the cutoff energy set to 400 eV. All calculations were considered converged when the total energy changed by less than 10^{-6} eV and interatomic forces were less than 0.02 eV/Å.

The Pt(111) surface was modelled using a p(4×4) supercell with a four layer thick slab where the bottom two layers of the surface were fixed into their bulk positions and the top two layers were allowed to relax. The vacuum distance was 15.1 Å. All zero Kelvin surface optimizations used a Gamma centered **k**-point mesh of (4×4×1). The Pt lattice constant was optimized using a Gamma point centered **k**-point mesh of (20×20×20) and found to be 3.979 Å. Structure visualization was performed with VESTA [33].

The adsorption energies of each two molecule system on Pt(111) was calculated according to Eq. (4):

$$E_{ads}^{X-Y} = E(X-Y/Pt) - E(Pt) - E(X) - E(Y) \quad (4)$$

where $E(X-Y/Pt)$, $E(Pt)$, $E(X)$, and $E(Y)$ are the total energies of adsorbed two molecule system (where X, Y can be AA, PA, GA and/or H_2O), Pt(111) slab and isolated gas phase molecules, respectively. The adsorption energies calculated here were under gas phase conditions. The effect of solvation on the adsorption energies was estimated using the bond additivity model of Singh and Campbell [34]. With this approach (details provided in the Supplementary Information, Fig. S8 and Table S2), we estimate that the shift from gas phase to aqueous phase stabilizes the adsorption energies of AA, PA and GA dimers on Pt (111) by −0.05, −0.07 and −0.15 eV, respectively, which is consistent with adsorption free energy differences between gas phase and aqueous phase conditions obtained from implicit solvation methods for PA on Ni (111), Pd(211), Rh(111), and Cu(111) by Heyden et al. [35–38] and both explicit and implicit solvation model results by Getman et al. [39]. Overall, we expect that the trends in adsorption energies for carboxylic acids on Pt(111) calculated here under gas phase conditions are directly transferable to aqueous phase conditions.

Further energetic analyses are performed by calculating the interaction energy of the two molecule adsorbed systems relative to their isolated adsorption energies, according to Eq. (5) and Eq. (6):

$$E_{ads}^{isolated} = E(X/Pt) - E(Pt) - E(X) \quad (5)$$

$$E_{interaction} = E_{ads}^{X-Y} - E_{ads}^{isolated}(X) - E_{ads}^{isolated}(Y) \quad (6)$$

If $E_{interaction}$ is positive (negative), then the intermolecular lateral interactions between adsorbates are repulsive (attractive). With this approach, we are able to quantify the nanoscale energetic driving forces for competitive adsorption between AA, PA, GA and H_2O.

The charge transfer between the dimer carboxylic acid configurations and Pt(111) upon adsorption was determined by calculating the differential charge density as defined by Eq. (7):

$$\Delta\rho = \rho(X-Y/Pt) - \rho(Pt) - \rho(X-Y) \quad (7)$$

Where $\rho(X-Y/Pt)$, $\rho(Pt)$, and $\rho(X-Y)$ are the charge distributions for the optimized structure of the adsorbed dimer system, the surface and gas phase dimer fixed in their adsorption geometries, respectively.

3. Results and discussion

3.1. Catalyst characterization

Textural properties of the catalyst were evaluated by nitrogen physisorption. As depicted in Fig. 1A, the isotherm profile could be referred to type I and type IV with regards to IUPAC classification, suggesting the presence of micropores and macropores structures [40]. BET surface area was equal to 1086 m^2/g, with 501 m^2/g attributed to micropore area. The total pore volume was found equal to 0.746 cm^3/g (0.242 cm^3/g micropore volume), while the average pore size was equal to 5.1 nm.

XRD patterns were recorded to investigate both the structural properties and mean crystal size for the fresh catalysts (Fig. 1B). The diffraction peak at 2θ of 25° was associated with the (002) plane of the

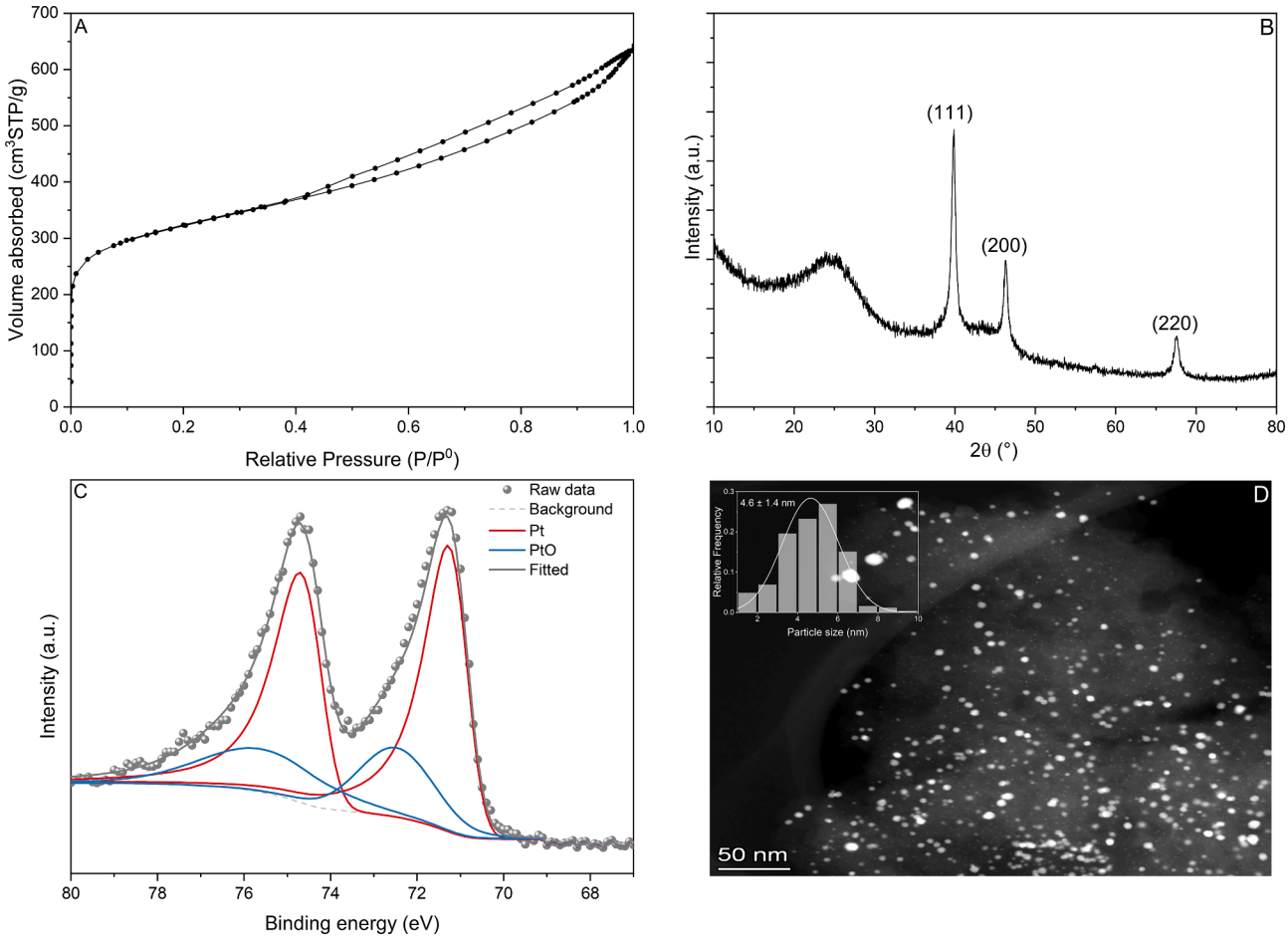

Fig. 1. N_2 adsorption/desorption isotherms (A), XRD patterns (B), XPS spectra (C), HAADF-STEM image and particles distribution (D) of the fresh catalyst.

hexagonal structure characteristic of carbon black. Pt^0 nanoparticles were crystalline, as indicated by the characteristic peaks at 2θ of 39.8, 46.3 and 67.6, associated with (111), (200) and (220) lattice planes, respectively.

Surface chemistry of Pt nanoparticles was evaluated by XPS, and the high-resolution spectrum is reported in Fig. 1C. The band in Pt4f was well explained by using the asymmetric peaks associated to Pt^0 and the peaks associated to Pt^{2+} (i.e., PtO). By the quantification of the phases, it was derived that metallic Pt accounted for the majority of the surface (73.2 %).

Finally, HAADF-STEM image (Fig. 1D) was analyzed showing that the average Pt particle size was equal to 4.6 nm, with a standard deviation equal to 1.4 nm. This result is apparently in contrast with the XRD analysis, where the presence of a sharp diffraction peak at 39.8° seemed to suggest a large size of Pt nanoparticles. However, this can be due to the presence of large agglomerates, as also observed by EDX mapping (Fig. S2). The dominant facets expected for Pt nanoparticles of this size are ~50 % (111), ~35 % (100), and ~15 % (110) [41]. The dominance of flat facets for Pt nanoparticles within our size range supports our choice of the (111) facet in our modelling work.

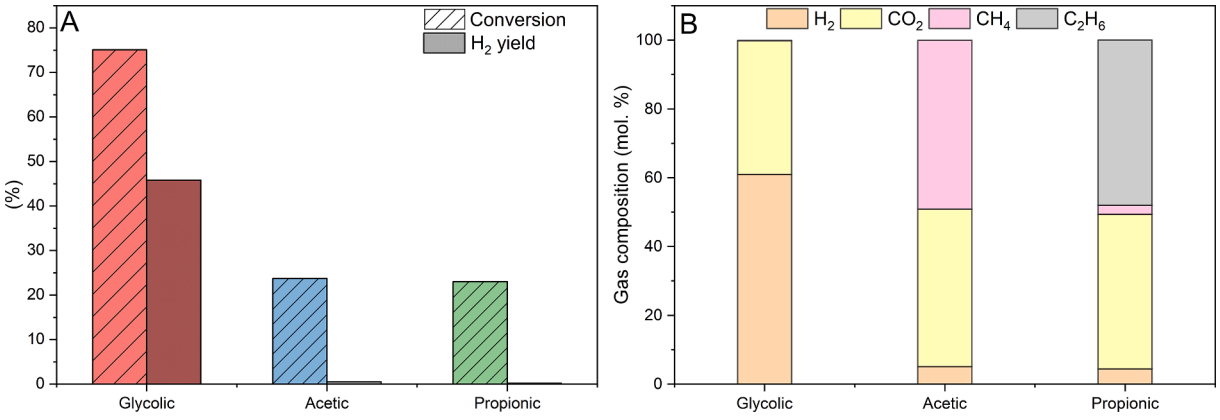

Fig. 2. Influence of the catalyst on APR of mono-component solution: A) Conversion and H_2 yield; B) Gas composition. Reaction conditions: 75 mL solution, 270 °C, 0.15 g catalyst, 1 h.

3.2. Mono-component solution

Preliminary tests were conducted on mono-component solutions of the model compounds. Fig. 2 depicts the catalytic performance of GA, AA and PA solutions in terms of conversion, hydrogen yield and gas composition. The outcomes here are important as they serve as an experimental basis for the successive DFT evaluation and for the interpretation of the non-linear phenomena observed in the case of multi-component mixtures.

GA showed the highest conversion among the three carboxylic acids, reaching 75 %, as well as the highest hydrogen yield, 45 % (Fig. 2A). In the liquid phase, only AA was found as a minor by-product, and it could be derived from the hydrogenation of the hydroxyl group due to the in-situ production of hydrogen, see Eq. (8). As reported in Fig. 2B, the gas phase is constituted by hydrogen and carbon dioxide, in fair accordance with the APR stoichiometry, see Eq. (9). It is important to note the key role played here by the Pt metal. In fact, a blank test carried out with only activated carbon led to just 5 % glycolic conversion.

$$Glycolic\ acid + H_2 \rightarrow Acetic\ acid + H_2O \quad (8)$$

$$Glycolic\ acid + H_2O \rightarrow 3H_2 + 2CO_2 \quad (9)$$

AA reported a much lower conversion, ca. 24 %, with negligible hydrogen production. This result suggests that AA is slightly activated under the present reaction conditions, but the reaction pathway does not foresee its reforming. This is confirmed by the analysis of the gas phase, where carbon dioxide and methane were equally present, suggesting that a catalytic decomposition occurred, see Eq. (10). In the liquid phase, no other products were detected.

$$Acetic\ acid \rightarrow CH_4 + CO_2 \quad (10)$$

Similarly to AA, PA reported a quite low conversion (about 23 %) and null hydrogen yield. However, in this case, the gas phase consisted mostly of ethane and carbon dioxide. This outcome indicates a common behaviour for PA and AA, specifically the occurrence of C-C bond breaking and decarboxylation reactions when starting from carboxylic acids, see Eq. (11).

$$Propionic\ acid \rightarrow C_2H_6 + CO_2 \quad (11)$$

The influence of initial concentration on the rate of consumption was assessed to determine the apparent reaction order (Fig. S3). As depicted in Fig. 3, each compound presented a reaction order lower than one.

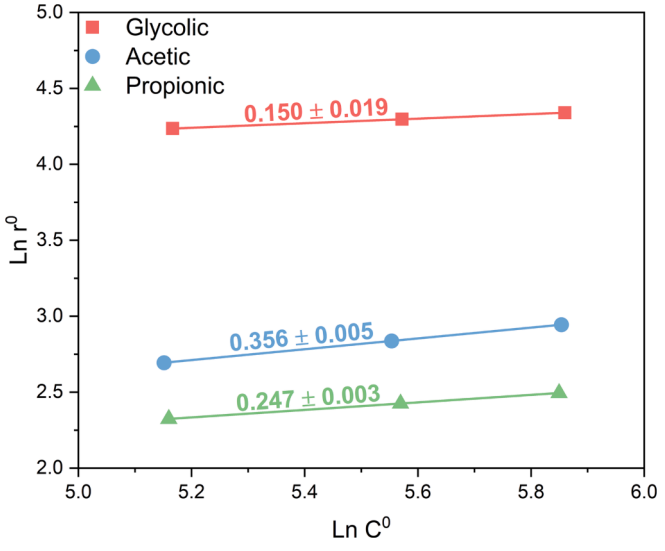

Fig. 3. Influence of feed concentration on the initial rate of consumption. Reaction conditions: 75 mL solution, 270 °C, 0.05/0.15 g 5 % Pt/C.

Such an outcome can be attributed to strong adsorption on the Pt surface, which leads to high surface coverage of the molecules even at low concentration (range 175–351 mmol/L). Low reaction orders are common for liquid phase reactions. For example, Shabaker et al. reported nearly first order (0.8) for methanol APR in the 1–10 wt% range on Pt surfaces, and 0.3 for ethylene glycol [42]. Interestingly, it can be observed that GA showed the lowest reaction order, suggesting a higher degree of saturation of the active sites with respect to the other carboxylic acids. This outcome supported the DFT modelling for the description of a saturated active site, with a high fraction of monolayer. It is worthy to note that, given the low reaction order, the kinetic behaviour of the molecules could be described by a Langmuir-Hinshelwood model, in which the adsorption term in the denominator plays a prevalent role. However, a full kinetic investigation is out of the scope of the present work, and it will be explored in a proper experimental campaign.

The existing computational studies for carboxylic acid adsorption on Pt(111) consider only isolated molecule adsorption, which is inconsistent with experimental observations [43–51]. The adsorbate-adsorbate lateral interactions, which can be repulsive or attractive, present under the high coverages representative of reaction conditions can significantly influence adsorption structures, reaction energies, and reaction pathways [52]. Modelling studies that do not account for such lateral interactions risk developing inaccurate pictures of adsorption and reaction, especially in systems where lateral interactions are substantial [53]. Thus, accounting for lateral interactions is critical to understanding the adsorption of AA, PA and GA on Pt(111).

Fig. 4 shows the adsorption energy for 0.0625 and 0.1250 ML of AA, PA and GA on Pt(111). Isolated (i.e., 0.0625 ML) AA and PA molecules are adsorbed onto the most favourable, upright sites identified from literature [43–46,48,50,51]. As GA adsorption on transition metal surfaces has been less studied [47,49], we performed configuration testing to identify the dominant GA adsorption configuration at 0.0625 ML (Fig. S4). For the 0.1250 ML coverage, AA was taken as an exemplar adsorbate for all acids studied here and 11 configurations were tested (Fig. S4). Overall, we find that increasing AA coverage causes a shift in configuration towards dimers. Thus, two configurations were tested for the 0.1250 ML coverage for all acids (Fig. S5): (1) upright and (2) dimer.

Starting with 0.0625 ML (Fig. 4A), our DFT results show that there is no substantial difference in the adsorption energies for AA, PA and GA (i.e., max difference ± 0.05 eV from our results). This is consistent with results from Salciccioli et al. (AA and PA/Pt(111)) [43] and Yan et al. (GA/Pt(111)) [47,49]. Moving to the 0.1250 ML upright structures, small lateral interactions appear, with AA-AA and PA-PA having repulsive interactions of ~47.9 and ~67.2 meV respectively while GA-GA has attractive interactions of 53.3 meV (Fig. 4B). These lateral interactions cause the adsorption energy differences present at 0.0625 ML to balance out and become identical for all acids (Fig. 4A). Thus, the results obtained for the upright adsorption configurations examined exclusively in the existing literature do not properly account for the adsorption discrepancies found experimentally.

Experimental surface science studies [54,55] for AA adsorption on Pt (111) suggest that AA-AA dimers form at moderate to high coverages. Thus, we examined a second, dimer configuration of each carboxylic acid at 0.1250 ML. Our DFT results show that the dimer structures are more stable—with stronger adsorption energies as compared to the upright configuration by 0.06, 0.20 and 0.33 eV for AA, PA and GA, respectively—on Pt(111) for all carboxylic acids (Fig. 4A). Intermolecular hydrogen bonding interactions between the carboxylic acid functionalities on neighbouring molecules produce attractive and stabilizing effects (Fig. 4B). Furthermore, the strength of these interactions increases markedly as we move from AA to PA to GA, indicating that the stability of the dimers is highly structure-dependent. Increasing the carbon chain length increases the attractive interaction energy in PA-PA dimers by approximately double as compared to AA-AA dimers. Meanwhile, the addition of the terminal hydroxyl functionality in GA

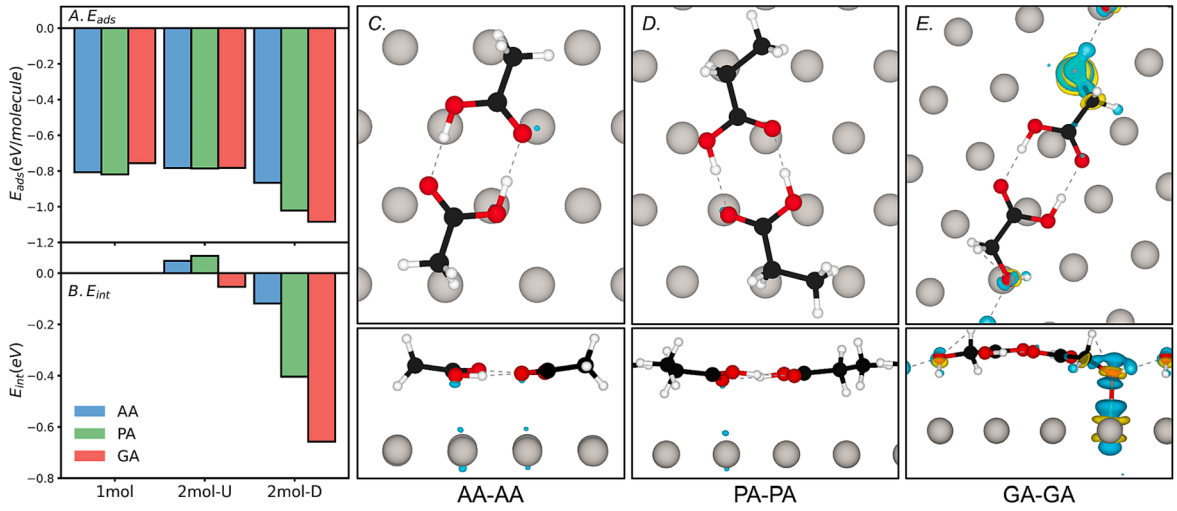

Fig. 4. (A) Average adsorption energy and (B) interaction energy for 0.0625 ML (1 mol) and 0.1250 ML (2 mol), upright (U) and dimer (D) configurations, of each carboxylic acid (i.e., AA, PA and GA) on Pt(1 1 1). (C)-(E) Top and side views of the differential charge density of each carboxylic acid dimer on Pt(1 1 1). The silver, red, black and white spheres represent Pt, O, C and H, respectively. Blue (yellow) isosurface colors show charge density gain (loss), with the isosurface level set to 0.004 e^{-}/Bohr^3. (For interpretation of the references to colour in this figure legend, the reader is referred to the web version of this article.)

increases the degree of intermolecular hydrogen bonding, resulting in interaction energies for GA-GA dimers that are more than double that of the PA-PA dimers and almost 7 times stronger than the AA-AA dimers.

We examined the effect of acid coverage and configuration on the reaction energy for initial O-H scission for all acids on Pt(111) and compared the resulting trends in reaction energy to those discussed with our existing trends for adsorption energy. Previous work for carboxylic acid reaction on transition metal surfaces identifies O-H scission on the carboxyl functionality to be the first elementary reaction step [35–38,45,46,48,50]. As shown in Fig. S6, the change from upright to dimer structure inverts the O-H scission reaction energies from exothermic to endothermic, indicating the dimer structures will be slower to react. Furthermore, the trend in O-H scission reaction energy follows GA > PA > AA. Thus, these results indicate that the reaction favorability of elementary reactions after adsorption will inherit an inversed trend to that seen in adsorption for the dimer structures identified here.

The underlying driving forces for carboxylic dimer adsorption on Pt (111) can be visualized through the differential charge densities during adsorption (Fig. 4C through E). For the AA-AA and PA-PA dimers (Fig. 4C and D), the differential charge densities show negligible charge transfer between the surface and dimers during adsorption. Thus, the adsorption and interaction energy differences caused by the change in carbon chain length result from purely van der Waals forces. Meanwhile, the differential charge density for the GA-GA dimer (Fig. 4E) shows significant charge transfer between the surface and a terminal hydroxyl functionality. This indicates that the increased stability of GA-GA dimers results from a combination of van der Waals and charge transfer effects. Fig. S7 depicts the adsorption of these carboxylic acids in the dimer configuration with intermolecular effects excluded by using the RPBE functional [56]. Without intermolecular attraction/repulsion, the pure attraction of these carboxylic acid dimers to the catalyst surface varies by only 0.04 eV. Thus, only when we incorporate the van der Waals forces and charges transferred (through the optB88-vdW functional) can we get results that explain the experimentally determined performance (Fig. 2) and rate orders (Fig. 3).

Other possible influences on the experimentally observed competitive adsorption effects were considered here: (1) solvent stabilization, (2) dehydrogenation via proton-electron transfer (PET) mechanisms at the water-Pt interface [57,58]. First, the influence of solvent stabilization on the DFT-based adsorption energy trends observed here was considered and found to be minimal and systematic for similarly structured adsorbates (see Table S2 and Fig. S8) [35–39]. Second, as the stability of PET transition states is highly dependent on the charge on the adsorbates and the ability of the adsorbate-covered surface to accept/donate electrons [59–62], we have performed Bader charge and work function calculations on our pure AA, PA and GA dimers on Pt(111). As shown in Table S3, Bader charge results suggest that the oxygen-bonded hydrogen in all acids can be exchanged with protons in the solvent water molecules without simultaneous electron transfer, while the carbon-bonded hydrogen in all acids could potentially be abstracted from the acid via a PET mechanism. The stability of such an interfacial proton, and thus the favourability of the PET mechanism, will depend on the work function of the adsorbate-covered surface. Shangguan et al. showed that a decrease in work function of 0.5 eV due to adsorbate type and coverage effects decreases the stability of interfacial protons generated under thermal conditions by ~0.5 eV [59]. As shown in Table S3, carboxylic acid adsorption on Pt(111) decreases the surface work function by 0.47–0.69 eV, which impedes electron transfer into the metal surface and destabilizes interfacial proton formation via PET mechanisms. Additionally, we can exclude the role that pH may have in driving the observed phenomena, as this issue may play a role in other contexts [63]. In fact, the initial pH was very close for each acid (between 2.1 and 2.6, at 176 mmol/L) and hence it would not reasonably explain such strong differences. Overall, we see that the influence of solvation either through stabilization, pH, or PET mechanisms is systematic between the three acids studied here, meaning that the trends in adsorption energy for AA, PA and GA dimers on Pt(111) are unchanged from gas phase to aqueous phase.

Taken together, our experimental and theoretical results on the mono-component systems show that there are notable performance dependencies for carboxylic acid conversion based on the chemical structure. While GA, PA and AA all experience high surface coverages based on the near zero rate orders, the conversion trends as GA > PA > AA. This trend in conversion is mirrored in the changes in adsorption and intermolecular interaction energies for each carboxylic acid on Pt (111), but only once the critical, high coverage dimer configuration was determined. We note that the modelling performed here is not sufficient to identify the degree of rate control [64] as such an analysis requires complete mapping of the potential energy surfaces, which is beyond the scope of this work. However, we see that the trend in acid adsorption strength is inherited and inverted by the reaction energies for subsequent elementary steps (i.e. O-H scission), suggesting that competitive adsorption is a crucial step for understanding the catalytic upgrading of

carboxylic acid mixtures. In the following section, we examine the APR catalytic performance and competitive adsorption effects of bi-component solutions of our three model carboxylic acids over Pt catalysts.

3.3. Bi-component solution

The successive step was performing the APR of binary solutions. Three mixtures were chosen, accordingly with the compounds used in the mono-component test: (i) GA and AA, (ii) PA and AA, (iii) GA and PA. The tests were performed over 5 % Pt/C using different molar ratios between the two compounds. In Table 1, the adopted nomenclature is linked to the substrates amount, to facilitate the understanding of the results.

3.3.1. Acetic acid and glycolic acid

The conversion of binary GA-AA mixtures is shown in Fig. 5. As discussed in Section 3.2, the mono-component AA solution showed 24 % conversion. When GA was added to the AA solution, in a 1:4 M ratio (G0.25A1), the AA conversion strongly decreased from 23.7 to 2.4 %. When the GA-AA ratio gradually increased to 1:1, the AA conversion decreased to −8.1 %. Please note that the apparent negative conversion of AA, and hence its production, is due to the GA side-reaction discussed in Section 3.2 (Eq. (8)). The GA conversion also decreased, from 100 % to 67.5 %, in the binary solutions, which can be attributed to the low reaction order of glycolic acid (Fig. 3).

To quantify more precisely the relative conversion of GA and AA, given that AA is a by-product of the APR of GA, the amount of methane produced from the binary mixtures was tracked. Methane was produced only marginally (0.03 mmol) by GA alone (Fig. 2B), while it was obtained as a main product by AA (2.55 mmol). Thus, methane is a useful probe molecule to follow the conversion path of AA. We observed that in G1A1, 0.11 mmol of methane were obtained; this value increased up to 0.40 mmol in G0.25A1. Therefore, it may be inferred that AA was gradually converted. If we try to estimate the AA conversion from the information on methane production, AA conversion declined from 3.1 % to 0.4 % moving from G0.25A1 to G1A1.

The dramatic drop in AA conversion is indicative of the strong adsorption of GA on the active metal compared to AA and cannot only be ascribed to the higher reactivity of GA. One way to understand this result is to examine the individual steps occurring in heterogeneous catalysis: diffusion through the bulk, diffusion into the pores, adsorption, surface reaction, and desorption of the products. Being in the kinetic regime, we can assume that the first two steps are fast for each component of the mixture. Then, we must discriminate if the adsorption is critical for AA

Table 1
Nomenclature used for the APR tests in the binary solutions.

Name	Glycolic ac. amount (mmol)	Acetic ac. amount (mmol)	Propionic ac. amount (mmol)
G0A1	0	13.2	0
G0.25A1	3.3	13.2	0
G0.5A1	6.6	13.2	0
G0.75A1	9.9	13.2	0
G1A1	13.2	13.2	0
G1A0	13.2	0	0
P0A1	0	13.2	0
P0.25A1	0	13.2	3.3
P0.5A1	0	13.2	6.6
P0.75A1	0	13.2	9.9
P1A1	0	13.2	13.2
P1A0	0	0	13.2
G0P1	0	0	13.2
G0.25P1	3.3	0	13.2
G0.5P1	6.6	0	13.2
G0.75P1	9.9	0	13.2
G1P1	13.2	0	13.2
G1P0	13.2	0	0

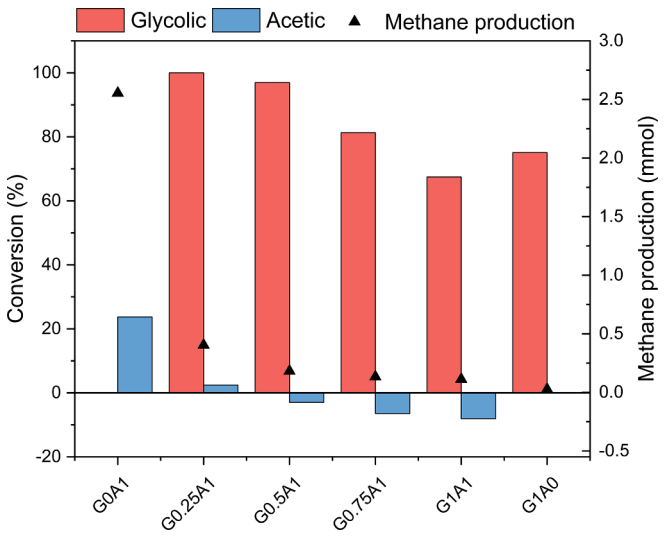

Fig. 5. Influence of solution composition on substrate conversion and methane production. Reaction conditions: 75 mL solution, 270 °C, 0.15 g 5 % Pt/C, 1 h.

conversion. If GA does not affect the surface coverage of AA, i.e., if their adsorption constants are similar, then we would expect that the concentrations on the catalyst surface reflect the solution composition, with AA being 4-fold more present than GA. At this point, being in the kinetic regime, we may assume that the conversion is proportional to the "available" active sites, which are 4/5 of the one in the mono-component solution. Therefore, the theoretical AA conversion should be about 19 %. The discrepancy with the experimental value should hence be caused by competitive adsorption phenomena, such as AA displacement from Pt sites when other molecules more affine with the active site are present in the solution. This behaviour is scarcely studied in literature for aqueous systems [65,66], and it is sometimes cited in the APR field without a deeper investigation [19].

Even though it is not possible to derive a global reaction order for GA from the results reported in Fig. 5, it seems that the GA conversion is still affected by a low reaction order. For example, by comparing the G0.5A1 and G1A1 test, GA conversion halved while its concentration doubled. We may infer that the dependency of the conversion rate from the initial concentration remain the same between the mono-component and multi-component mixtures, in accordance with the results observed in other catalytic reactions in liquid phase [66–68].

The time behaviour of AA and GA in some selected conditions is reported in Fig. 6. In the AA mono-component solution (Fig. 6A), its conversion steadily increased with the reaction time reaching 38 % as final value. When 3.3 mmoles of GA were added, a drastic drop was observed, so that the final conversion was 5 %, more than 7-fold lower than the mono-component case. The conversion was inversely proportional to the GA concentration, eventually reaching 0.3 %, but moving through negative values during the reaction, due to the parallel GA hydrogenation. These results confirm the competition on the active sites between AA and GA, with the latter having significantly higher affinity than the former on the Pt surface.

GA conversion reached 100 % after 0.5 h in the most diluted case, while it took 2 h in the G0.5A1 run. This outcome affected the AA fate because it had more time to convert in the former case, since no more GA was present in the solution after 0.5 h. Moreover, the lower GA concentration led to less AA by-product production. Despite this, the AA conversion was lower than expected. It is not possible to provide a definitive reason for this result: we suggest that it may compete with the adsorption of other by-products, such as CO, which are strongly adsorbed on Pt [69]. Further work will be performed to evaluate this hypothesis.

GA out-competing AA for available surface sites on the Pt catalyst is

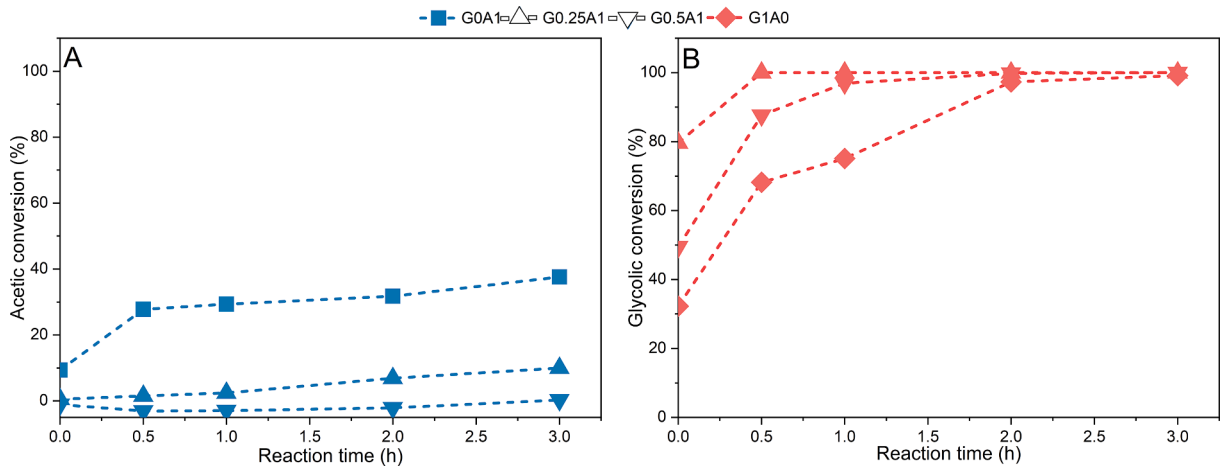

Fig. 6. Influence of reaction time on AA (A) and GA (B) conversion. Reaction conditions: 75 mL solution, 270 °C, 0.15 g 5 % Pt/C.

consistent with the stronger adsorption energy and stronger, attractive intermolecular lateral interactions present in GA dimers as compared to AA dimers on Pt(111), as shown in Fig. 4. However, the DFT results in the pure AA-AA, PA-PA and GA-GA dimers do not include consideration of mixed dimer structures between AA-PA, AA-GA and PA-GA, as well as neglecting the impact of the aqueous environment through consideration of H_2O-AA, H_2O-PA and H_2O-GA dimers. The adsorption and interaction energies for such mixed systems are examined here and shown in Fig. 7 (AA-PA, AA-GA and PA-GA) and Fig. S8 (H_2O-AA, H_2O-PA and H_2O-GA). The water-acid adsorption and interaction energies are all notably weak. Thus, the presence of water is not expected to significantly impact the trends in carboxylic acid adsorption on Pt(111). Furthermore, the mixed 0.1250 ML upright configurations show no impact of the carboxylic acid chemical structure on the adsorption energy with minimal lateral effects (i.e., less than ~30 meV attractive interactions for GA-AA and GA-PA, and outright ~82 meV repulsive interactions for PA-AA). This is consistent with the pure carboxylic acid 0.1250 ML upright configuration results.

For AA-GA mixtures, there are noticeable interaction energies for the mixed 0.1250 ML dimers. The interaction energies for AA-GA mixed dimers were determined to be ~ −0.2 eV (Fig. 7B). This, when compared to the interaction energies of the pure AA-AA and GA-GA dimers shows that incorporation of AA into the adsorbed dimer has an antagonistic effect. Thus, the DFT results are consistent with the experimental observations and further support the proposed picture of competitive adsorption being the dominant factor here.

3.3.2. Acetic acid and propionic acid

Fig. 8 shows the influence of the feed composition on the conversion of PA and AA binary mixtures. Adding 3.3 mmol of PA to the mono-component AA solution decreased the AA conversion only to a small extent in this case, from 23.7 % to 17.6 %; afterwards, the gradual addition of the second carboxylic acid led to the final conversion equal to 5.2 %, while the conversion of PA was 22.4 %. This value was slightly lower than the mono-component solution (P1A0), where the conversion was ca. 23 %.

These results allowed us to derive some information regarding the behaviour of mixtures under APR conditions. PA has a similar reactivity with AA in the mono-component solution; however, it has a higher conversion than AA in the equimolar run (P1A1), indicating that it may outcompete AA for adsorption sites and, thus, overall allowing it to be more reactive. Furthermore, AA is gradually inhibited by the presence of

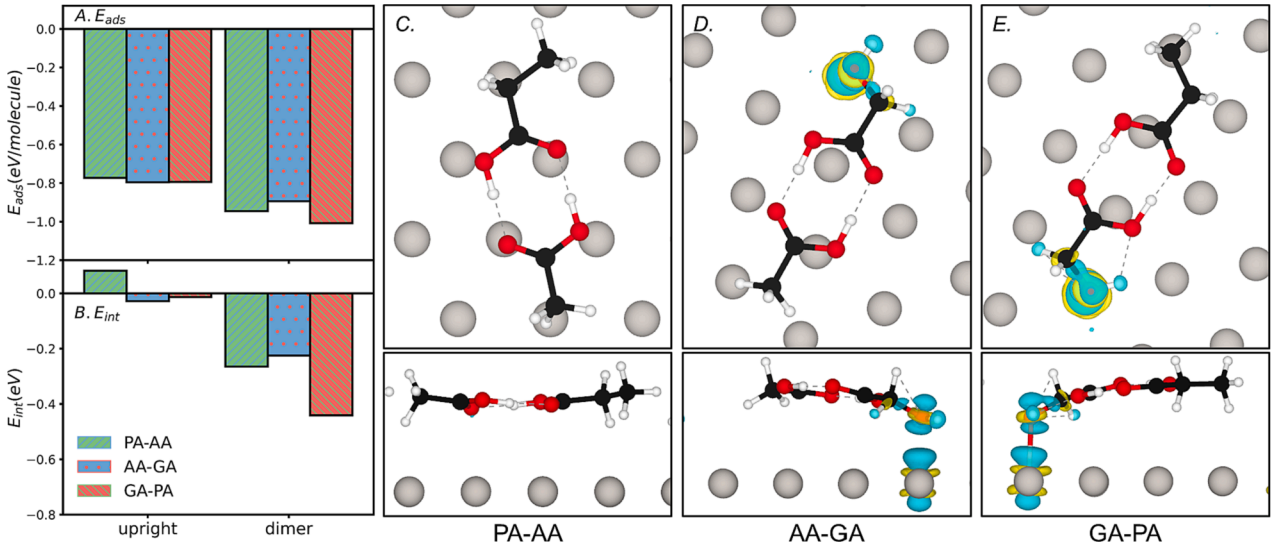

Fig. 7. *(A) Average adsorption energy and (B) interaction energy for 0.1250 ML, upright (U) and dimer (D) configurations, of carboxylic acid mixtures on Pt(1 1 1). (C)-(E) Top and side views of the differential charge density of each mixed carboxylic acid dimer on Pt(1 1 1). The silver, red, black, and spheres represent Pt, O, C, and respectively. Blue (yellow) isosurface colors show charge density gain (loss), with the isosurface level set to 0.004 e^-/Bohr^3.* (For interpretation of the references to colour in this figure legend, the reader is referred to the web version of this article.)

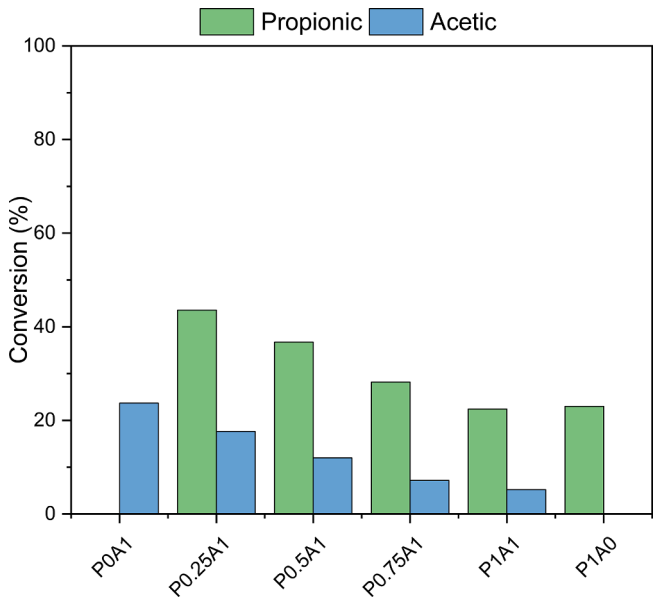

Fig. 8. Influence of solution composition on substrates conversion. Reaction conditions: 75 mL solution, 270 °C, 0.15 g 5 % Pt/C, 1 h.

PA, even if to a less extent compared to GA.

The influence of reaction time on AA and PA conversion for some selected runs is reported in Fig. 9. With respect to AA conversion (Fig. 9A), it could be observed that the presence of PA slowed down its conversion at each reaction time (–32 % after 3 h), likely due to less available active sites due to the co-adsorption of PA. However, this occurrence is significantly less severe than in the case of GA co-adsorption, where, in the G0.25A1 mixture, the AA conversion dropped by 87 %. On the other hand, PA conversion (Fig. 9B) increased in the binary mixture, likely due to the low reaction order, as reported above.

From the pure component dimer DFT-based adsorption energies (Fig. 4), we expect PA to outcompete AA for available sites given the stronger adsorption energy and attractive intermolecular lateral interactions present in PA dimers as compared to AA dimers on Pt(111). Examination of AA-PA mixed dimers on Pt(111) shows the interaction energies to be ~ −0.3 eV, which is a purely additive effect. Furthermore, as the PA-AA dimer has a weaker adsorption energy than pure PA-PA dimers, PA is expected to predominantly outcompete AA in such a binary mixture.

3.3.3. Glycolic acid and propionic acid

Given the stronger adsorption energy of PA with respect to AA, GA-PA binary mixtures were investigated to understand to what extent the latter may have better performance in the multi-component scenario. Fig. 10 shows that the addition of GA to the PA solution (G0.25P1) decreased its conversion by 71 % (from to 23 % to ca. 7 %), with an almost complete conversion of GA. This result is similar to the outcome reported for the AA-GA mixture, indicating the higher affinity of GA on Pt sites with respect to PA. However, the extent of this competition is less severe here with respect to the AA-GA case, where the AA conversion dropped by 87 %.

The addition of GA to the bi-component mixture gradually decreased its conversion, as well as that of PA, which reached a final conversion of ca. 2 % in the equimolar solution. Again, this value is significantly higher than the AA conversion, which was only 0.4 %, suggesting its higher extent of adsorption. Furthermore, this outcome can be observed by the higher drop in the GA conversion moving from the mono-component solution to the equimolar one: while it was by only 10 % in the AA-GA solution, here it is up to 33 %.

From the pure component dimer DFT-based adsorption energies (Fig. 4), we expect GA to outcompete PA for available sites given the

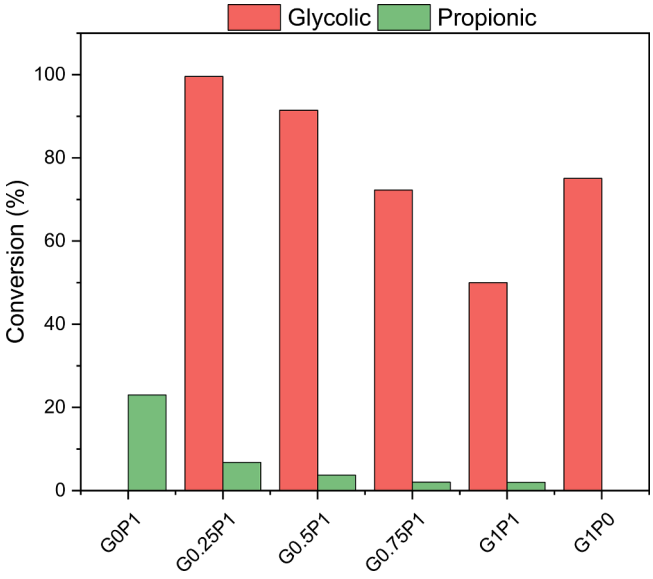

Fig. 10. Influence of solution composition on substrate conversion. Reaction conditions: 75 mL solution, 270 °C, 0.15 g 5 % Pt/C, 1 h.

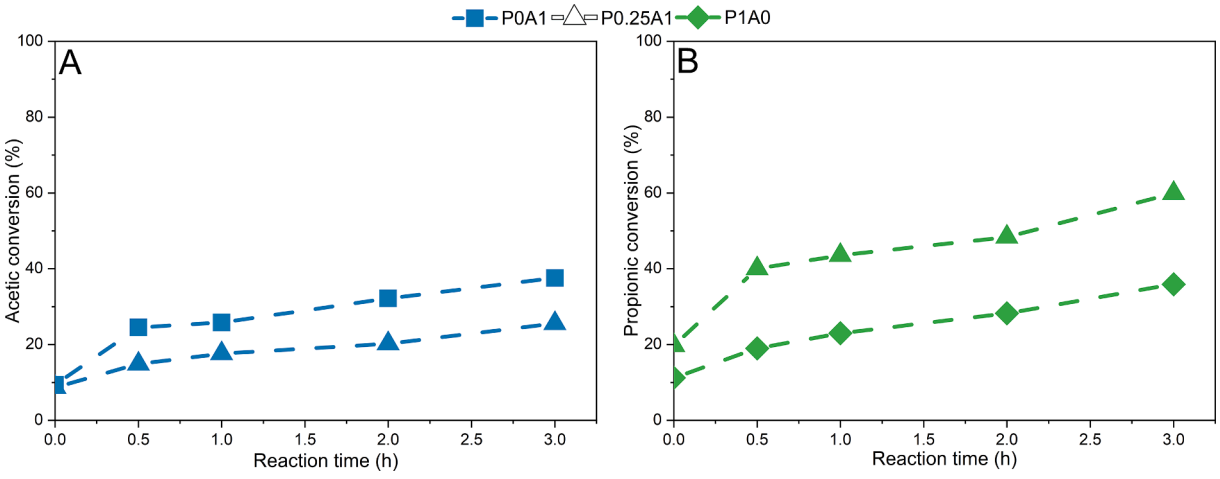

Fig. 9. Influence of reaction time on AA (left) and PA (right) conversion. Reaction conditions: 75 mL solution, 270 °C, 0.15 g 5 % Pt/C.

stronger adsorption energy and attractive intermolecular lateral interactions present in GA dimers as compared to PA dimers on Pt(111). Examination of GA-PA mixed dimers on Pt(111) shows the interaction energies to be ~ −0.4 eV, which is a purely additive effect. This shows that PA has an antagonistic impact on the overall dimer adsorption strength, consistent with the decrease in charge transfer between dimer and surface in GA-PA dimers (Fig. 7) as compared to GA-GA dimers (Fig. 4). Overall, the DFT results are consistent with the experimental conversion results and competitive adsorption interpretation.

3.3.4. Perspective

Overall, our combined experimental and theoretical approach rationalizes the changes in catalytic performance for multi-component carboxylic acid systems relative to their mono-component systems with competitive adsorption. While adsorption alone is rarely a rate determining step, it is important for setting the overall coverage and availability of surface sites. Particularly in mixed feedstocks, the competitive adsorption between various reactants will consequently affect what is bound to the surface and can undergo subsequent elementary surface reactions. If one reactant within a mixture sees a significantly stronger adsorption energy than others, this reactant will dominate the available adsorption sites, blocking other reactants from interacting with the catalyst. Thus, characterizing and understanding competitive adsorption effects becomes critical to rationalizing catalytic observations for complex feedstock mixtures.

Here, the underlying driving force for the performance difference due to competitive adsorption was changes in the intermolecular interactions within the dominant, high coverage dimer configuration that carboxylic acids form on the Pt catalyst surface. Using the PA-AA binary mixtures as an example, the conversion of AA in the mixture fell below the conversion observed for pure AA due to the strong adsorption energies resulting from stronger intermolecular interactions within PA-PA dimers (~ −0.40 eV) compared to AA-AA dimers (~ −0.11 eV) and PA-AA dimers (~ −0.26 eV). Furthermore, whenever binary mixtures comprise GA, there is a substantially greater surface-adsorbate interaction between GA and the Pt catalyst in the form of charge transfer as compared to AA or PA. This, together with the stronger interaction energies of GA in its pure dimers (~ −0.7 eV) than the interaction energies of binary multicomponent mixtures, ensures that GA dominates the catalytic surface in the presence of other acids.

Fig. 11 illustrates the hypothetical temporal evolution of an example system of GA-AA system with an excess of AA. In stage 1, the Pt surface was clean, while in the solution there was an excess of AA compared to GA. During stage 2, despite the higher AA concentration, the stronger adsorption energy resulting from greater attractive lateral interactions led to higher GA surface coverage, which started to react (stage 3), producing hydrogen and carbon dioxide. Furthermore, new GA molecules adsorbed on the Pt which were set free by the desorption of the products. When GA was (almost) completely converted, AA was eventually able to find available sites to react. Further research on catalyst design should look at dopants able to improve the adsorption ability of such molecules.

4. Conclusion

In this study, APR of a model corn stover HTL-WW was performed in a batch reactor to derive experimental and theoretical information on competitive adsorption phenomena in binary carboxylic acid mixtures. GA, AA and PA, representatives of the most common species present in the HTL-WW, were investigated alone and in mixtures to get an insight on their reactivities with a 5 % Pt/C, their affinities with the active sites, and their relative influences between the molecules. Thanks to a detailed characterization of both liquid and gas phase products, it was observed that AA conversion was more susceptible to competition with GA rather than with PA. The strong adsorption of GA was confirmed by the kinetic analysis, which reported the lowest rate dependence on the initial reactant concentration. DFT modelling showed that the adsorption strengths of the carboxylic acids on Pt(111) trended as GA > PA > AA. These trends are determined by the strong, attractive intermolecular interactions between carboxylic acids at higher coverages, causing the acids to preferentially adsorb into dimer structures. Furthermore, examination of mixed acid dimers (i.e., GA-AA, PA-AA) showed there to be an antagonistic effect that further suppresses the adsorption of AA relative to PA and GA.

The insights gained from this work can prompt future research in active catalysts for carboxylic acid activation. The results emphasize the crucial need to investigate representative mixtures due to the occurrence of intense competitive adsorption phenomena, whose understanding is essential for advancing the field and ensuring the effectiveness of these processes. Further research on effective dopants able to enhance the adsorption ability of recalcitrant molecules should be addressed. Furthermore, studies on the solvent effects should be developed, for its interaction with reactants/products as well as the competition for the adsorption on the active sites.

CRediT authorship contribution statement

Giuseppe Pipitone: Conceptualization, Data curation, Formal analysis, Investigation, Methodology, Writing – original draft, Writing – review & editing. **Alyssa J.R. Hensley:** Conceptualization, Data curation, Formal analysis, Funding acquisition, Investigation, Methodology, Software, Supervision, Writing – original draft, Writing – review &

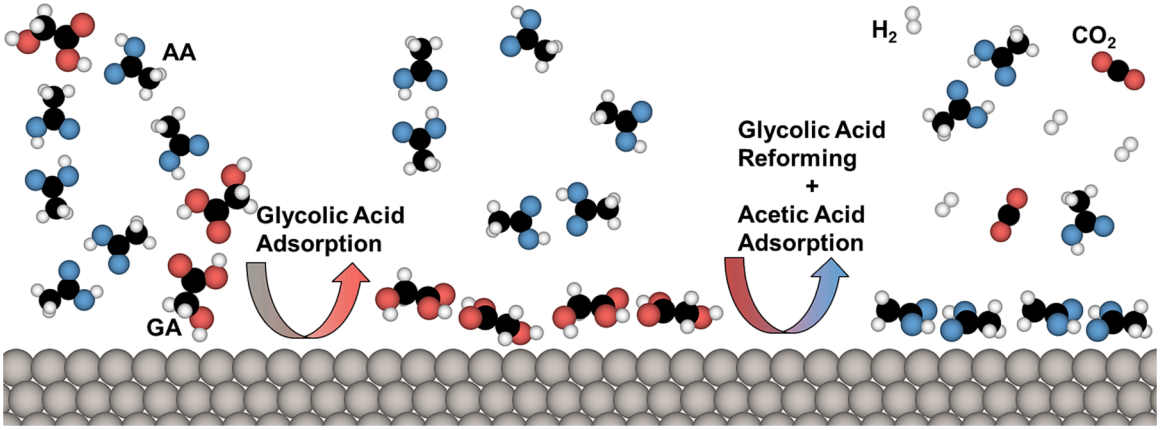

Fig. 11. Illustrative description of the adsorption between AA and GA on Pt surface. The silver, blue, pink, black and white spheres represent Pt, O (acetic acid), O (glycolic acid), C and H, respectively. (For interpretation of the references to colour in this figure legend, the reader is referred to the web version of this article.)

editing. **Ayodeji Omoniyi:** Data curation, Formal analysis, Investigation, Software, Writing – original draft. **Giulia Zoppi:** Conceptualization, Investigation, Methodology, Writing – review & editing. **Raffaele Pirone:** Conceptualization, Project administration, Supervision. **Samir Bensaid:** Conceptualization, Funding acquisition, Project administration, Supervision.

Declaration of competing interest

The authors declare that they have no known competing financial interests or personal relationships that could have appeared to influence the work reported in this paper.

Data availability

Data will be made available on request.

Acknowledgments

This work was supported by institutional funds provided to A.J.R.H. from the Department of Chemical Engineering and Materials Science at Stevens Institute of Technology. Computational resources were obtained from the Center for Nanoscale Materials. Work performed at the Center for Nanoscale Materials, a U.S. Department of Energy Office of Science User Facility, was supported by the U.S. DOE, Office of Basic Energy Sciences, under Contract No. DE-AC02-06CH11357. G.P. and S.B. acknowledge PNRR M4C2, Investimento 1.4 – Avviso n. 3138 del 16/12/2021 – CN00000013 National Centre for HPC, Big Data and Quantum Computing (HPC) – CUP E13C22000990001. Dr. Eleonora Calì is gratefully acknowledged for the TEM characterization.

Appendix A. Supplementary data

Supplementary data to this article can be found online at https://doi.org/10.1016/j.cej.2024.148902.

References

[1] ONU The Sustainable Development Agenda Available online: https://www.un.org/sustainabledevelopment/development-agenda/.
[2] P. Kehrein, M. Van Loosdrecht, P. Osseweijer, M. Garfí, J. Dewulf, J. Posada, A Critical Review of Resource Recovery from Municipal Wastewater Treatment Plants-Market Supply Potentials, Technologies and Bottlenecks, Environ. Sci. Water Res. Technol. 6 (2020) 877–910, https://doi.org/10.1039/c9ew00905a.
[3] L. Grande, I. Pedroarena, S.A. Korili, A. Gil, Hydrothermal Liquefaction of Biomass as One of the Most Promising Alternatives for the Synthesis of Advanced Liquid Biofuels: A Review, Materials (basel). 14 (2021) 5286, https://doi.org/10.3390/ma14185286.
[4] S.D. Davidson, J.A. Lopez-Ruiz, Y. Zhu, A.R. Cooper, K.O. Albrecht, R.A. Dagle, Strategies to Valorize the Hydrothermal Liquefaction-Derived Aqueous Phase into Fuels and Chemicals, ACS Sustain. Chem. Eng. 7 (2019) 19889–19901, https://doi.org/10.1021/acssuschemeng.9b05308.
[5] A. Swetha, S. Shrivigneshwar, K. Panchamoorthy, R. Sivaramakrishnan, R. Shanmuganathan, J. Arun, Review on Hydrothermal Liquefaction Aqueous Phase as a Valuable Resource for Biofuels, Bio-Hydrogen and Valuable Bio-Chemicals Recovery. *Chemosphere* 283 (2021) 131248, https://doi.org/10.1016/j.chemosphere.2021.131248.
[6] R. Posmanik, R.A. Labatut, A.H. Kim, J.G. Usack, J.W. Tester, L.T. Angenent, Technology Coupling Hydrothermal Liquefaction and Anaerobic Digestion for Energy Valorization from Model Biomass Feedstocks, Bioresour. Technol. 233 (2017) 134–143, https://doi.org/10.1016/j.biortech.2017.02.095.
[7] S. Fernandez, K. Srinivas, A.J. Schmidt, M.S. Swita, B.K. Ahring, Anaerobic Digestion of Organic Fraction from Hydrothermal Liquefied Algae Wastewater Byproduct, Bioresour. Technol. 247 (2018) 250–258, https://doi.org/10.1016/j.biortech.2017.09.030.
[8] L. Zhang, P. Champagne, C. Xu Charles, Supercritical Water Gasification of an Aqueous By-Product from Biomass Hydrothermal Liquefaction with Novel Ru Modified Ni Catalysts, Bioresour. Technol. 102 (2011) 8279–8287, https://doi.org/10.1016/j.biortech.2011.06.051.
[9] Y. Li, W.A. Tarpeh, K.L. Nelson, T.J. Strathmann, Quantitative Evaluation of an Integrated System for Valorization of Wastewater Algae as Bio-Oil, Fuel Gas, and Fertilizer Products, Environ. Sci. Technol. 52 (2018) 12717–12727, https://doi.org/10.1021/acs.est.8b04035.
[10] J. Watson, T. Wang, B. Si, W.T. Chen, A. Aierzhati, Y. Zhang, Valorization of Hydrothermal Liquefaction Aqueous Phase: Pathways towards Commercial Viability, Prog. Energy Combust. Sci. 77 (2020) 100819, https://doi.org/10.1016/j.pecs.2019.100819.
[11] S. Poirier, O. Chapleur, Inhibition of Anaerobic Digestion by Phenol and Ammonia: Effect on Degradation Performances and Microbial Dynamics, Data Br. 19 (2018) 2235–2239, https://doi.org/10.1016/j.dib.2018.06.119.
[12] P. Sundarrajan, K.P. Gopinath, J. Arun, K. Gracepavithra, A.A. Joseph, S. Manasa, Insights into Valuing the Aqueous Phase Derived from Hydrothermal Liquefaction, Renew. Sustain. Energy Rev. 144 (2021) 111019, https://doi.org/10.1016/j.rser.2021.111019.
[13] L. Leng, W. Zhang, S. Leng, J. Chen, L. Yang, H. Li, S. Jiang, H. Huang, Bioenergy Recovery from Wastewater Produced by Hydrothermal Processing Biomass: Progress, Challenges, and Opportunities, Sci. Total Environ. 748 (2020) 142383, https://doi.org/10.1016/j.scitotenv.2020.142383.
[14] R.D. Cortright, R.R. Davda, J.A. Dumesic, Hydrogen from Catalytic Reforming of Biomass-Derived Hydrocarbons in Liquid Water, Nature 418 (2002) 964–967, https://doi.org/10.1038/nature01009.
[15] I. Coronado, M. Stekrova, M. Reinikainen, P. Simell, L. Lefferts, J. Lehtonen, A Review of Catalytic Aqueous-Phase Reforming of Oxygenated Hydrocarbons Derived from Biorefinery Water Fractions, Int. J. Hydrogen Energy 41 (2016) 11003–11032, https://doi.org/10.1016/j.ijhydene.2016.05.032.
[16] A. Kirilin, J. Wärnå, A. Tokarev, D.Y. Murzin, Kinetic Modeling of Sorbitol Aqueous-Phase Reforming over Pt/Al 2O3, Ind. Eng. Chem. Res. 53 (2014) 4580–4588, https://doi.org/10.1021/ie403813y.
[17] D.Y. Murzin, S. Garcia, V. Russo, T. Kilpiö, L.I. Godina, A.V. Tokarev, A.V. Kirilin, I. L. Simakova, S. Poulston, D.A. Sladkovskiy, et al., Kinetics, Modeling, and Process Design of Hydrogen Production by Aqueous Phase Reforming of Xylitol, Ind. Eng. Chem. Res. 56 (2017) 13240–13253, https://doi.org/10.1021/acs.iecr.7b01636.
[18] F. Aiouache, L. McAleer, Q. Gan, A.H. Al-Muhtaseb, M.N. Ahmad, Path Lumping Kinetic Model for Aqueous Phase Reforming of Sorbitol, Appl. Catal. A Gen. 466 (2013) 240–255, https://doi.org/10.1016/j.apcata.2013.06.039.
[19] I. Coronado, A. Arandia, M. Reinikainen, R. Karinen, R.L. Puurunen, J. Lehtonen, Kinetic Modelling of the Aqueous-Phase Reforming of Fischer-Tropsch Water over Ceria-Zirconia Supported Nickel-Copper Catalyst, Catalysts 9 (2019) 936, https://doi.org/10.3390/catal9110936.
[20] G. Pipitone, G. Zoppi, R. Pirone, S. Bensaid, A Critical Review on Catalyst Design for Aqueous Phase Reforming, Int. J. Hydrogen Energy 47 (2022) 151–180, https://doi.org/10.1016/j.ijhydene.2021.09.206.
[21] B. Maddi, E. Panisko, T. Wietsma, T. Lemmon, M. Swita, K. Albrecht, D. Howe, Quantitative Characterization of the Aqueous Fraction from Hydrothermal Liquefaction of Algae, Biomass and Bioenergy 93 (2016) 122–130, https://doi.org/10.1016/j.biombioe.2016.07.010.
[22] B. Maddi, E. Panisko, T. Wietsma, T. Lemmon, M. Swita, K. Albrecht, D. Howe, Quantitative Characterization of Aqueous Byproducts from Hydrothermal Liquefaction of Municipal Wastes, Food Industry Wastes, and Biomass Grown on Waste, ACS Sustain. Chem. Eng. 5 (2017) 2205–2214, https://doi.org/10.1021/acssuschemeng.6b02367.
[23] E. Panisko, T. Wietsma, T. Lemmon, K. Albrecht, D. Howe, Characterization of the Aqueous Fractions from Hydrotreatment and Hydrothermal Liquefaction of Lignocellulosic Feedstocks, Biomass and Bioenergy 74 (2015) 162–171, https://doi.org/10.1016/j.biombioe.2015.01.011.
[24] U.S. Billi, US Billion Ton Update: Biomass Supply for a Bioenergy and Bioproducts Industry (Executive Summary), Ind. Biotechnol. 7 (2011) 375–380, https://doi.org/10.1089/ind.2011.7.375.
[25] G. Pipitone, G. Zoppi, S. Ansaloni, S. Bocchini, F.A. Deorsola, R. Pirone, S. Bensaid, Towards the Sustainable Hydrogen Production by Catalytic Conversion of C-Laden Biorefinery Aqueous Streams, Chem. Eng. J. 377 (2019) 120677, https://doi.org/10.1016/j.cej.2018.12.137.
[26] G. Kresse, J. Hafner, Ab Initio Molecular Dynamics for Liquid Metals, Phys. Rev. B 47 (1993) 558–561, https://doi.org/10.1103/PhysRevB.47.558.
[27] G. Kresse, J. Furthmüller, Efficient Iterative Schemes for Ab Initio Total-Energy Calculations Using a Plane-Wave Basis Set, Phys. Rev. B - Condens. Matter Mater. Phys. 54 (1996) 11169–11186, https://doi.org/10.1103/PhysRevB.54.11169.
[28] P.E. Blöchl, Projector Augmented-Wave Method, Phys. Rev. B 50 (1994) 17953–17979, https://doi.org/10.1103/PhysRevB.50.17953.
[29] G. Kresse, D. Joubert, From Ultrasoft Pseudopotentials to the Projector Augmented-Wave Method, Phys. Rev. B - Condens. Matter Mater. Phys. 59 (1999) 1758–1775, https://doi.org/10.1103/PhysRevB.59.1758.
[30] J. Klimeš, D.R. Bowler, A. Michaelides, Chemical Accuracy for the van Der Waals Density Functional, J. Phys. Condens. Matter 22 (2010), https://doi.org/10.1088/0953-8984/22/2/022201.
[31] J. Klimeš, D.R. Bowler, A. Michaelides, Van Der Waals Density Functionals Applied to Solids, Phys. Rev. B - Condens. Matter Mater. Phys. 83 (2011) 1–13, https://doi.org/10.1103/PhysRevB.83.195131.
[32] M. Methfessel, A.T. Paxton, High-Precision Sampling for Brillouin-Zone Integration in Metals, Phys. Rev. B 40 (1989) 3616–3621, https://doi.org/10.1103/PhysRevB.40.3616.
[33] K. Momma, F. Izumi, VESTA 3 for Three-Dimensional Visualization of Crystal, Volumetric and Morphology Data, J. Appl. Crystallogr. 44 (2011) 1272–1276, https://doi.org/10.1107/S0021889811038970.
[34] N. Singh, C.T. Campbell, A Simple Bond-Additivity Model Explains Large Decreases in Heats of Adsorption in Solvents Versus Gas Phase: A Case Study with Phenol on Pt(111) in Water, ACS Catal. 8116–8127 (2019), https://doi.org/10.1021/acscatal.9b01870.

[35] M. Zare, R.V. Solomon, W. Yang, A. Yonge, A. Heyden, Theoretical Investigation of Solvent Effects on the Hydrodeoxygenation of Propionic Acid over a Ni(111) Catalyst Model, J. Phys. Chem. C 124 (2020) 16488–16500, https://doi.org/10.1021/acs.jpcc.0c04437.
[36] S. Behtash, J. Lu, O. Mamun, C.T. Williams, J.R. Monnier, A. Heyden, Solvation Effects in the Hydrodeoxygenation of Propanoic Acid over a Model Pd(211) Catalyst, J. Phys. Chem. C 120 (2016) 2724–2736, https://doi.org/10.1021/acs.jpcc.5b10419.
[37] W. Yang, R.V. Solomon, O. Mamun, J.Q. Bond, A. Heyden, Investigation of the Reaction Mechanism of the Hydrodeoxygenation of Propionic Acid over a Rh(1 1 1) Surface: A First Principles Study, J. Catal. 391 (2020) 98–110, https://doi.org/10.1016/j.jcat.2020.08.015.
[38] B. Rajbanshi, W. Yang, A. Yonge, S.K. Kundu, C. Fricke, A. Heyden, Computational Investigation of the Catalytic Hydrodeoxygenation of Propanoic Acid over a Cu (111) Surface, J. Phys. Chem. C 125 (2021) 19276–19293, https://doi.org/10.1021/acs.jpcc.1c05240.
[39] X. Zhang, R.S. Defever, S. Sarupria, R.B. Getman, Free Energies of Catalytic Species Adsorbed to Pt(111) Surfaces under Liquid Solvent Calculated Using Classical and Quantum Approaches, J. Chem. Inf. Model. 59 (2019) 2190–2198, https://doi.org/10.1021/acs.jcim.9b00089.
[40] N. Mojoudi, N. Mirghaffari, M. Soleimani, H. Shariatmadari, C. Belver, J. Bedia, Phenol Adsorption on High Microporous Activated Carbons Prepared from Oily Sludge: Equilibrium, Kinetic and Thermodynamic Studies. *Sci. Rep.* 9 (2019) 1–12, https://doi.org/10.1038/s41598-019-55794-4.
[41] R. Ding, I.M. Padilla Espinosa, D. Loevlie, S. Azadehranjbar, A.J. Baker, G. Mpourmpakis, A. Martini, T.D.B. Jacobs, Size-Dependent Shape Distributions of Platinum Nanoparticles, Nanoscale Adv. 4 (2022) 3978–3986, https://doi.org/10.1039/d2na00326k.
[42] J.W. Shabaker, R.R. Davda, G.W. Huber, R.D. Cortright, J.A. Dumesic, Aqueous-Phase Reforming of Methanol and Ethylene Glycol over Alumina-Supported Platinum Catalysts, J. Catal. 215 (2003) 344–352, https://doi.org/10.1016/S0021-9517(03)00032-0.
[43] M. Salciccioli, S.M. Edie, D.G. Vlachos, Adsorption of Acid, Ester, and Ether Functional Groups on Pt: Fast Prediction of Thermochemical Properties of Adsorbed Oxygenates via DFT-Based Group Additivity Methods, J. Phys. Chem. C 116 (2012) 1873–1886, https://doi.org/10.1021/jp2091413.
[44] R. Alcala, J.W. Shabaker, G.W. Huber, M.A. Sanchez-Castillo, J.A. Dumesic, Experimental and DFT Studies of the Conversion of Ethanol and Acetic Acid on PtSn-Based Catalysts, J. Phys. Chem. B 109 (2005) 2074–2085, https://doi.org/10.1021/jp049354t.
[45] M.S. Hofman, E.V. Scoullos, J.P. Robbins, L. Ezeonu, D.V. Potapenko, X. Yang, S. G. Podkolzin, B.E. Koel, Acetic Acid Adsorption and Reactions on Ni(110), Langmuir 36 (2020) 8705–8715, https://doi.org/10.1021/acs.langmuir.0c00713.
[46] K.C. Chukwu, L. Árnadóttir, Density Functional Theory Study of Decarboxylation and Decarbonylation of Acetic Acid on Pd(111), J. Phys. Chem. C 124 (2020) 13082–13093, https://doi.org/10.1021/acs.jpcc.0c00436.
[47] H. Yan, S. Yao, W. Liang, X. Feng, X. Jin, Y. Liu, X. Chen, C. Yang, Selective Oxidation of Glycerol to Carboxylic Acids on Pt(111) in Base-Free Medium: A Periodic Density Functional Theory Investigation, Appl. Surf. Sci. 497 (2019) 143661, https://doi.org/10.1016/j.apsusc.2019.143661.
[48] Y.X. Ran, Z.Y. Du, Y.P. Guo, J. Feng, W.Y. Li, Density Functional Theory Study of Acetic Acid Steam Reforming on Ni(111), Appl. Surf. Sci. 400 (2017) 97–109, https://doi.org/10.1016/j.apsusc.2016.12.148.
[49] H. Yan, S. Yao, J. Wang, S. Zhao, Y. Sun, M. Liu, X. Zhou, G. Zhang, X. Jin, X. Feng, et al., Engineering Pt-Mn2O3 Interface to Boost Selective Oxidation of Ethylene Glycol to Glycolic Acid, Appl. Catal. B Environ. 284 (2021), https://doi.org/10.1016/j.apcatb.2020.119803.
[50] R.S. Shamsiev, I.E. Sokolov, F.O. Danilov, V.R. Flid, Theoretical Study of the Mechanism of Propionic Acid Deoxygenation on the Palladium Surface, Kinet. Catal. 60 (2019) 627–634, https://doi.org/10.1134/S0023158419050094.
[51] J. Lu, M. Faheem, S. Behtash, A. Heyden, Theoretical Investigation of the Decarboxylation and Decarbonylation Mechanism of Propanoic Acid over a Ru(0 0 0 1) Model Surface, J. Catal. 324 (2015) 14–24, https://doi.org/10.1016/j.jcat.2015.01.005.
[52] M. Saeys, M.F. Reyniers, G.B. Marin, M. Neurock, Density Functional Study of Benzene Adsorption on Pt(111), J. Phys. Chem. B 106 (2002), https://doi.org/10.1021/jp0201231.
[53] T. Panczyk, P. Szabelski, The Influence of Lateral Interactions between Adsorbed Molecules on Adsorption Kinetics. A Statistical Rate Theory Approach, J. Phys. Chem. B 107 (2003) 5586–5597, https://doi.org/10.1021/jp034354z.
[54] Q. Gao, J.C. Hemminger, Chemisorption and Thermal Decomposition of Acetic Acid on Pt(111), J. Electron Spectros. Relat. Phenomena 54–55 (1990) 667–676, https://doi.org/10.1016/0368-2048(90)80259-D.
[55] Q. Gao, J.C. Hemminger, A Vibrational Spectroscopy Study of CH3COOH, CH3COOD and 13CD3COOH(D) Adsorption on Pt(111). I. Surface Dimer Formation and Hydrogen Bonding, Surf. Sci. 248 (1991) 45–56, https://doi.org/10.1016/0039-6028(91)90060-6.
[56] B. Hammer, L.B. Hansen, J.K. Nørskov, Improved Adsorption Energetics within Density-Functional Theory Using Revised Perdew-Burke-Ernzerhof Functionals, Phys. Rev. B - Condens. Matter Mater. Phys. 59 (1999) 7413–7421, https://doi.org/10.1103/PhysRevB.59.7413.
[57] T.S. Wesley, Y. Román-Leshkov, Y. Surendranath, Spontaneous Electric Fields Play a Key Role in Thermochemical Catalysis at Metal-Liquid Interfaces, ACS Cent. Sci. 7 (2021) 1045–1055, https://doi.org/10.1021/acscentsci.1c00293.
[58] P. Huang, Y. Yan, A. Banerjee, L. Lefferts, B. Wang, J.A. Faria Albanese, Proton Shuttling Flattens the Energy Landscape of Nitrite Catalytic Reduction, J. Catal. 413 (2022) 252–263, https://doi.org/10.1016/j.jcat.2022.06.007.
[59] J. Shangguan, A.J.R. Hensley, L. Morgenstern, Z. Li, J.S. McEwen, W. Ma, Y. H. (Cathy) Chin, Brønsted Acidity of H-Adatoms at Protic Solvent-Transition Metal Interfaces and Its Kinetic Consequences in Electrophilic Addition Reactions, J. Catal. 408 (2022) 179–195, https://doi.org/10.1016/j.jcat.2021.12.003.
[60] Hensley, A.J.R.; Bray, J.; Shangguan, J.; Chin, Y.H. (Cathy); McEwen, J.S. Catalytic Consequences of Hydrogen Addition Events and Solvent-Adsorbate Interactions during Guaiacol-H2 Reactions at the H2O-Ru(0 0 0 1) Interface. *J. Catal.* **2021**, *395*, 467–482, doi:10.1016/j.jcat.2020.09.034.
[61] J. Shangguan, A.J.R. Hensley, M.V. Gradiski, N. Pfriem, J.S. McEwen, R.H. Morris, Y.H.C. Chin, The Role of Protons and Hydrides in the Catalytic Hydrogenolysis of Guaiacol at the Ruthenium Nanoparticle-Water Interface, ACS Catal. 10 (2020) 12310–12332, https://doi.org/10.1021/acscatal.0c01963.
[62] G. Cheng, A. Jentys, O.Y. Gutiérrez, Y. Liu, Y.H. (Cathy) Chin, J.A. Lercher, Critical Role of Solvent-Modulated Hydrogen-Binding Strength in the Catalytic Hydrogenation of Benzaldehyde on Palladium, Nat. Catal. 4 (2021), https://doi.org/10.1038/s41929-021-00701-2.
[63] B. Saenz de Miera, A.S. Oliveira, J.A. Baeza, L. Calvo, J.J. Rodriguez, M. A. Gilarranz, Treatment and Valorisation of Fruit Juice Wastewater by Aqueous Phase Reforming: Effect of PH, Organic Load and Salinity, J. Clean. Prod. 252 (2020) 119849, https://doi.org/10.1016/j.jclepro.2019.119849.
[64] C.T. Campbell, The Degree of Rate Control: A Powerful Tool for Catalysis Research, ACS Catal. 7 (2017) 2770–2779, https://doi.org/10.1021/acscatal.7b00115.
[65] F.T. Jere, J.E. Jackson, D.J. Miller, Kinetics of the Aqueous-Phase Hydrogenation of L -Alanine to L -Alaninol, Ind. Eng. Chem. Res. 43 (2004) 3297–3303.
[66] Y. Chen, D.J. Miller, J.E. Jackson, Kinetics of Aqueous-Phase Hydrogenation of Organic Acids and Their Mixtures over Carbon Supported Ruthenium Catalyst, Ind. Eng. Chem. Res. 46 (2007) 3334–3340, https://doi.org/10.1021/ie0614632.
[67] M.S. Lylykangas, P.A. Rautanen, A.O.I. Krause, Liquid-Phase Hydrogenation Kinetics of Multicomponent Aromatic Mixtures on Ni/Al2O3, Ind. Eng. Chem. Res. 41 (2002) 5632–5639, https://doi.org/10.1021/ie0202930.
[68] J. Zhang, B. Hou, A. Wang, Z. Li, H. Wang, T. Zhang, Kinetic Study of the Competitive Hydrogenation of Glycolaldehyde and Glucose on Ru/C with or without AMT, AIChE J. 61 (2015), https://doi.org/10.1002/aic.14639.
[69] P.J. Dietrich, T. Wu, A. Sumer, J.A. Dumesic, J. Jellinek, W.N. Delgass, F. H. Ribeiro, J.T. Miller, Aqueous Phase Glycerol Reforming with Pt and PtMo Bimetallic Nanoparticle Catalysts: The Role of the Mo Promoter, Top. Catal. 56 (2013) 1814–1828, https://doi.org/10.1007/s11244-013-0115-1.